Tau impairs neural circuits, dominating amyloid-β effects, in Alzheimer models *in vivo*

Authors: Marc Aurel Busche[1,2*], Susanne Wegmann[1,3], Simon Dujardin[1], Caitlin Commins[1], Julia Schiantarelli[1], Naomi Klickstein[1], Tarun V. Kamath[1], George A. Carlson[4], Israel Nelken[5], and Bradley T. Hyman[1,*]

Affiliations:

[1]MassGeneral Institute for Neurodegenerative Disease, Massachusetts General Hospital, Harvard Medical School, Charlestown, Massachusetts, USA

[2]UK Dementia Research Institute at University College London, London, UK

[3]German Center for Neurodegenerative Diseases (DZNE), Berlin, Germany

[4]McLaughlin Research Institute, Great Falls, Montana, USA

[5]Department of Neurobiology, Silberman Institute of Life Sciences and Edmond and Lily Safra Center for Brain Sciences, Hebrew University of Jerusalem, Jerusalem, Israel

*Correspondence to: bhyman@mgh.harvard.edu or m.busche@ucl.ac.uk

The coexistence of amyloid-β (Aβ) plaques and tau neurofibrillary tangles (NFTs) in the neocortex is linked to neural system failure and cognitive decline in Alzheimer´s Disease (AD). However, the underlying neuronal mechanisms are unknown. By employing *in vivo* two-photon Ca^{2+}-imaging of layer 2/3 cortical neurons in mice expressing human Aβ and tau, we reveal a dramatic tau-dependent suppression of activity and silencing of many neurons, which dominates over Aβ-dependent neuronal hyperactivity. We show that NFTs are neither sufficient nor required for the silencing, which instead is dependent on soluble tau. Surprisingly, although rapidly effective in tau mice, suppression of tau gene expression was much less effective in rescuing neuronal impairments in mice containing both Aβ and tau.

Together, our results reveal how Aβ and tau synergize to impair the functional integrity of neural circuits *in vivo*, and suggest a possible cellular explanation contributing to disappointing results from anti-Aβ therapeutic trials.

The primary pathological hallmarks of Alzheimer´s Disease (AD) are extracellular plaques and intracellular NFTs[1]. The main component of plaques is the amyloid-β (Aβ) peptide, while NFTs are composed mainly of the protein tau. Autopsy and recent positron emission tomography (PET) studies revealed that the formation of plaques is spatially and temporally separated from that of NFTs: plaques first form in the neocortex and spread inwards to deeper brain regions, while NFTs first form in limbic areas, from where they spread outwards to the neocortex[2-4]. Several lines of evidence suggest that the propagation of tau pathology into the Aβ-plaques bearing cortex is linked to the transition from the preclinical ('asymptomatic') to the clinical ('symptomatic') stage of AD[5-7]. While previous studies have shown that the interaction between Aβ and tau causes enhanced pathology[6-14], the functional consequences for intact neuronal circuits remain unknown. To address this question, we employed *in vivo* two-photon Ca^{2+}-imaging of large populations of neurons in layer 2/3 of the neocortex in novel AD model mice that display spatially overlapping Aβ and tau pathologies in the cortex, similar to AD patients.

We began by monitoring action potential-related spontaneous Ca^{2+}-transients[15, 16] in GCaMP6f-expressing cortical layer 2/3 neurons of APPswe:PS1ΔE9 (APP/PS1) transgenic mice that overexpress human Aβ and develop only Aβ plaques (but no cytosolic tau pathology; APP/PS1 mice and all other mice used in this study are on the same FVBB6F1 genetic background, see Methods and Life Sciences Reporting Summary for details regarding the

breeding strategy). In agreement with previous results[17-20], we detected hyperactivity of layer 2/3 neurons in 6 to 12 months old plaque-bearing APP/PS1 mice (mean age 8.4 months, see also **Supplementary Figs. 1 and 2a** for details regarding age distributions and rationale for pooling functional neuronal data from mice at this 6- to 12-months age range) when compared to their wild-type controls (mean age 8.4 months; **Fig. 1a-h**). We then analyzed layer 2/3 neuronal activity in age-matched rTg4510 transgenic mice that express aggregating human tauP301L and display NFTs but no Aβ pathology (**Fig. 1c**). In stark contrast to the results obtained with APP/PS1 mice, in all 9/9 rTg4510 mice (mean age 8.4 months) examined, there was a strong reduction of cortical activity levels (**Fig. 1c-h**; linear mixed effects model for log(rates) on genetic background, $F(2,4351) = 132$, $P = 1.2e\text{-}56$; all *post hoc* comparisons between genotypes (controls, APP/PS1, rTg4510) were highly significant, $P < 10^{-6}$). Detailed analysis of all recorded neurons revealed that, relative to control and APP/PS1 mice, there was a 3.6- and 5.8-fold increase in the proportion of silent neurons in the rTg4510 mice (**Fig. 1i**), but virtually no neuronal hyperactivity (**Fig. 1h**). We then analyzed immunohistochemically stained brain sections from the imaged rTg4510 mice and found that NFTs were present only in 1.21 % of the GCamP6f-expressing cells (18/1483 cells double-positive for Alz50/PHF-1 and GFP; **Supplementary Fig. 3**), leading us to the hypothesis that aggregation of tau is not necessary for neuronal silencing. To test this hypothesis directly, we performed recordings in rTg21221 mice that overproduce non-aggregating wild-type human tau at comparable levels as rTg4510 mice but lack NFTs (**Fig. 2a, right panel, and Supplementary Figs. 4 and 5**). Indeed, **Figure 2b-e** shows that, similar to rTg4510 mice (**Fig. 1**), in 6 to 12 month old rTg21221 mice ($n = 6$; mean age 8.9 months) there was a marked reduction of layer 2/3 neuronal activity levels (linear

mixed effects model for log(rates) on genetic background, F(2,4494) = 183, *P* = 1.6e-77; *post hoc* multiple comparisons between genotypes were *P* < 0.0001), as well as a strong increase in the fractions of silent neurons (**Fig. 2e**). These results indicate that the impairment of neurons can occur independently of tau aggregation and NFT formation.

Having demonstrated that Aβ and tau alone have markedly opposite effects on the activity status of neurons, we next asked what is the net effect of Aβ and tau together. To address this question, we performed recordings in 6- to 12-months old APP/PS1 mice crossed with rTg4510 or rTg21221 mice[11, 21] (**Fig. 3a-c and Supplementary Fig. 6**). To our surprise, neuronal hyperactivity was not only completely abolished in the resulting APP/PS1-rTg4510 (*n* = 8; mean age 7.6 months) and APP/PS1-rTg21221 (*n* = 5; mean age 7.9 months) mice, but there was also a strong reduction in cortical activity levels (**Fig. 3d-j**; linear mixed effects model for log(rates) on genetic background, F(3,5558) = 671, *P* = 0; *post hoc* multiple comparisons between genotypes were all *P* < 2e-20). Further analysis revealed that, similar to rTg4510 and rTg21221 mice, abnormally silent neurons constitute a large pool of layer 2/3 neurons both in APP/PS1-rTg4510 as well as APP/PS1-rTg21221 mice (**Fig. 3k**). We independently obtained similar results in a 17- to 24-months old cohort of mice (mean age 20.6 months; **Supplementary Fig. 7**, see also **Supplementary Figs. 2b and 8** for more details on age distributions and rationale for pooling neuronal data from mice at this 17- to 24-months age range).

Given that the rTg4510 transgene is associated with an age-dependent loss of neurons which is even enhanced in the APP/PS1-rTg4510 crosses[11], potentially contributing to the observed functional impairments, we next analyzed young, 3- to 4-months old rTg4510 mice with and without the APP/PS1 transgene. This analysis revealed a strong reduction in neuronal

activities (significant effect of group: F(3,5594) = 14.9, *P* = 1.1e-9, *post hoc* analysis revealed significant differences between the APP/PS1-rTg4510 and all other groups), and increased fractions of silent layer 2/3 neurons in the APP/PS1-rTg4510 crosses already at this early disease stage, prior to overt neuropathology and neurodegeneration (**Supplementary Fig. 9**). **Supplementary Fig. 10** shows a comparison of the age-dependent changes of cortical neuronal activities for all genotypes. Together, these results indicate that tau blocks Aβ-dependent hyperactivity, resulting in a profound silencing of circuits when both Aβ and tau are present together in the cortex, and reinforcing the idea that NFTs are not critical for this suppression of neuronal activity.

Finally, we employed repeated two-photon Ca^{2+}-imaging and determined, in the same mice, whether impaired neuronal circuit function could be rescued by suppressing tau transgene expression. In these experiments, we took advantage of the fact that the tau mice used in this study were equipped with a regulatable promoter system, which allowed us to turn off the expression of the tau transgene by administration of a doxycycline (DOX)-containing diet, as demonstrated in several previous studies[22-24]. We carried out two-photon Ca^{2+}-imaging of layer 2/3 neurons in the same mice before and 6 weeks after DOX-treatment (all mice were at least six months of age when DOX treatment was started). We found that the neuronal impairments were apparently completely reversed in rTg21221 (*n* = 8) and also in rTg4510 (*n* = 7) mice (**Fig. 4a-e and Supplementary Fig. 11**), despite the continued presence of cortical NFTs (**Supplementary Fig. 12a-c)**. However, instead of the expected rescue of circuit impairment, in all 5/5 recorded APP/PS1-rTg4510 and all 5/5 recorded APP/PS1-rTg21221 mice there was no apparent change in the fractions of silent neurons after DOX-treatment (**Fig. 4b-h and**

Supplementary Fig. 11). The activity levels (**Fig. 4c,d and Fig. 4f,g**) showed a significant interaction between crossing with APP/PS1 and DOX-treatment for both rTg4510 and rTg21221 mice (linear mixed effects models for log(rates) on APP/PS1 crossing and DOX-treatment, rTg4510: interaction F(1,4615) = 49.0, $P = 2.8*10^{-12}$; *post hoc*, DOX-treatment increased significantly ($P < 0.05$) the activity level for both crossed and uncrossed strains, but the increase in activity levels for the crossed strain was significantly smaller – compare **Fig. 4c,f**; rTg21221: interaction F(1,3170) = 94, $P = 6.1*10^{-22}$; *post-hoc*, DOX-treatment significantly increased activity level in the uncrossed, but not in the crossed, strain – compare **Fig. 4d,g**). Importantly, the observation that tau suppression in the presence of Aβ was significantly less effective in restoring normal neuronal activities could not be explained by the degree of tau reduction, because enzyme-linked immunosorbent assay (ELISA) analysis showed significant and comparable reductions of total human tau levels upon DOX-treatment in all genotypes (**Supplementary Fig. 12d-g);** in line with previous reports[22], we also found that sarkosyl soluble tau levels, measured in forebrain homogenates of rTg4510 mice with and without the APP/PS1 transgene using Western blot, were reduced by DOX treatment, while sarkosyl-insoluble fractions were not significantly affected (**Supplementary Fig. 13**).

To determine if tau suppression would be effective in mice harboring tau and Aβ at an earlier age, prior to substantial neuropathology and neurodegeneration, we treated 3- to 4 months old rTg4510 mice with and without the APP/PS1 transgene with DOX for 6 weeks. **Supplementary Figure 14** shows that, while there was a significant reduction in the fractions of silent neurons in rTg4510 mice (significant effect of treatment, F(1,1388) = 28.1, $P = 1.3e-7$), in APP/PS1-rTg4510 crosses the fractions of silent neurons remained unchanged (no significant

effect of treatment, F(1,3195) = 0.47, *P* = 0.49). To show that the effects differed in the rTg4510 mice with and without the APP/PS1 transgene, we performed a linear mixed effects model. As expected, there were main effects of APP/PS1 crossing (F(1,4583) = 37.1, *P* = 1.2e-9) and of DOX-treatment (F(1,4583) = 29.0, *P* = 7.4e-8); importantly, the interaction was significant as well (F(1,4583) = 21.9, *P* = 2.9e-6), demonstrating that the difference between the effects of DOX-treatment in the young rTg4510 and APP/PS1-rTg4510 mice were highly significant. Again, ELISA analysis showed a substantial reduction in total human tau levels in all mice receiving DOX (**Supplementary Fig. 14e,f**). As a control, we treated wild-type control mice with DOX and found no significant effects (**Supplementary Fig. 15**; F(1,2686) = 0.589, *P* = 0.44).

In conclusion, our study reveals that the two major proteins involved in AD have dramatically opposing effects on the activity of neuronal circuits *in vivo*: Aβ alone causes hyperactivity, whereas tau alone suppresses activity and promotes silencing of many neurons. Remarkably, neuronal silencing dominates over hyperactivity when Aβ and tau are present together, as also corroborated by a recent *in vitro* study employing extracellular field recordings in entorhinal cortex slices[25]. The dramatic dominance of tau was, however, unexpected in light of previous studies suggesting that tau regulates, and is essential for, Aβ-dependent hyperexcitability[26-28]. While effects of transgene insertion must always be considered, the Aβ-induced hyperactivity phenotype is observed in multiple APP overexpressing lines with different transgene arrays[29] and is blocked by BACE inhibitors, which presumably impact primarily Aβ generation[20]; the tau phenotype is observed in two different tau transgenic lines that express two different tau transgenes (P301L or wild type) with substantially different age related histopathological phenotypes (aggregated tau and neurofibrillary tangles and

neurodegeneration in rTg4510, or not, in the rTg21221 line). Taken together with the observation that DOX suppression of the transgene ameliorates the abnormal physiology, we believe that the most parsimonious explanation for these observations is that Aβ and tau are responsible for the hyperactivity and suppressed baseline excitability observed in our study.

Our new results fit well with and provide a possible cellular explanation for the clinical observations that (i) AD patients exhibit a progressive decrease of whole-brain activity[30-32] and regional cerebral blood flow (rCBF)[33] as well as a slowing of the electroencephalogram (EEG)[34], and that (ii) tau, rather than Aβ, determines cognitive status[7, 35, 36]. The dominance of tau could also explain the relative lack of clinical improvement after Aβ suppression in recent clinical trials. In this context, it is noteworthy that AD carries an increased risk of epileptic seizures[37], and that several studies have shown increased activation of brain regions such as hippocampus using blood-oxygen level dependent (BOLD) functional magnetic resonance imaging (fMRI)[38, 39] (but see ref. [40]). To reconcile these observations with our new results it will be important to better understand the precise relationship between single-neuron and (abnormal) population activity. Nonetheless, as neuronal hyperactivity appears to be more related to Aβ[29], it is possible that epileptiform activity and BOLD-hyperactivation are more prominent in AD patients who have relatively higher Aβ than tau levels, i.e., at very early (possibly presymptomatic) points in the disease process when Aβ deposits occur throughout the cortex, but tangles are limited to medial temporal lobe. This appears to be the case for fMRI hyperactivity in the hippocampus[38]. Our finding that tau suppresses neuronal activity agrees with previous electrophysiological studies[41-43], and goes on to demonstrate that soluble, non-aggregated tau is sufficient for neuronal silencing, and that NFTs are not required. The link between soluble tau

and neuronal dysfunction may provide a mechanistic explanation for the observation that, in mouse models, cognitive deficits occur independently of NFT formation[22, 44-48]; that NFTs are not necessarily associated with functional impairments is also in line with previous studies showing that NFT-bearing cortical neurons can reliably respond to strong synaptic inputs, e.g. during simple sensory stimuli[49, 50]. Another unexpected but intriguing result of our study was the finding that suppression of tau gene expression rescued neuronal circuit impairments in tau mice, but was significantly less effective when Aβ was present at the same time. This lack of effect was present already in young mice, prior to substantial neuropathology, synapse loss and neurodegeneration, but nonetheless may be related to more severe and persisting synaptic and cellular changes in the context of (soluble) Aβ-tau interactions compared to Aβ or tau alone. Notably, the aggregated tau in NFTs is the target for several ongoing clinical trials; our current data argue that readouts for these trials need to be reconsidered as well. Together, our new results clarify the pathological role of interaction between Aβ and tau in impairing neuronal circuit integrity and function in AD, with important mechanistic and therapeutic implications not only for AD, but also for other tauopathies and other conditions that are associated with elevated tau.

ACKNOWLEDGEMENTS

We thank Ashley B. Robbins, Diana L. Corjuc, Allyson D. Roe and Eloise Hudry for excellent technical support; and all members of the Hyman laboratory for providing comments and advice throughout the project. We thank Matthias Staufenbiel for helpful discussions and experimental suggestions. We acknowledge the Genetically-Encoded Neuronal Indicator and Effector (GENIE) Project and the Janelia Farm Research Campus of the Howard Hughes Medical Institute and specifically V. Jayaraman, R.A. Kerr, D.S. Kim, L.L. Looger and K. Svoboda from the GENIE Project, Janelia Farm Research Campus, Howard Hughes Medical Institute for making AAV.Syn.GCaMP6f publicly available. We thank Dr. Peter Davies for kindly providing PHF-1 and Alz50 antibodies. We thank the following funding agencies for their support: M.A.B. was supported by an EMBO Long-Term Fellowship (ALTF 590-2016), the Alzheimer Forschung Initiative and the UK Dementia Research Institute. I.N. was supported by an advanced ERC grant (project RATLAND). B.T.H. received support from the Massachusetts Alzheimer Disease Research Center (P50AG005134), the JPB foundation, the NIH (1R01AG0586741) and the Tau Consortium.

AUTHOR CONTRIBUTIONS

M.A.B. and B.T.H. designed the study; M.A.B., S.W., S.D., C.C., J.S., N.K. and T.V.K. performed research; M.A.B., S.W., S.D., C.C. and I.N. analyzed data; G.A.C. provided background information regarding mouse breeding; M.A.B. and B.T.H. wrote the manuscript with input from all other authors.

COMPETING INTERESTS

The authors declare no competing financial interests related to this project.

REFERENCES

1. Hyman, B.T.*, et al.* National Institute on Aging-Alzheimer's Association guidelines for the neuropathologic assessment of Alzheimer's disease. *Alzheimers Dement* **8**, 1-13 (2012).

2. Braak, H. & Braak, E. Neuropathological stageing of Alzheimer-related changes. *Acta Neuropathol* **82**, 239-259 (1991).

3. Arnold, S.E., Hyman, B.T., Flory, J., Damasio, A.R. & Van Hoesen, G.W. The topographical and neuroanatomical distribution of neurofibrillary tangles and neuritic plaques in the cerebral cortex of patients with Alzheimer's disease. *Cereb Cortex* **1**, 103-116 (1991).

4. Scholl, M.*, et al.* PET imaging of tau deposition in the aging human brain. *Neuron* **89**, 971-982 (2016).

5. Delacourte, A.*, et al.* The biochemical pathway of neurofibrillary degeneration in aging and Alzheimer's disease. *Neurology* **52**, 1158-1165 (1999).

6. Wang, L.*, et al.* Evaluation of tau imaging in staging Alzheimer Disease and revealing interactions between β-amyloid and tauopathy. *JAMA Neurol* **73**, 1070-1077 (2016).

7. Pontecorvo, M.J.*, et al.* Relationships between flortaucipir PET tau binding and amyloid burden, clinical diagnosis, age and cognition. *Brain* **140**, 748-763 (2017).

8. Lewis, J.*, et al.* Enhanced neurofibrillary degeneration in transgenic mice expressing mutant tau and APP. *Science* **293**, 1487-1491 (2001).

9. Gotz, J., Chen, F., van Dorpe, J. & Nitsch, R.M. Formation of neurofibrillary tangles in P301l tau transgenic mice induced by Aβ 42 fibrils. *Science* **293**, 1491-1495 (2001).

10. Hurtado, D.E.*, et al.* Aβ accelerates the spatiotemporal progression of tau pathology and augments tau amyloidosis in an Alzheimer mouse model. *Am J Pathol* **177**, 1977-1988 (2010).

11. Bennett, R.E.*, et al.* Enhanced tau aggregation in the presence of amyloid β. *Am J Pathol* **187**, 1601-1612 (2017).

12. Jacobs, H.I.L.*, et al.* Structural tract alterations predict downstream tau accumulation in amyloid-positive older individuals. *Nat Neurosci* **21**, 424-431 (2018).

13. Quiroz, Y.T.*, et al.* Association between amyloid and tau accumulation in young adults with autosomal dominant Alzheimer Disease. *JAMA Neurol* **75**, 548-556 (2018).

14. He, Z.*, et al.* Amyloid-beta plaques enhance Alzheimer's brain tau-seeded pathologies by facilitating neuritic plaque tau aggregation. *Nat Med* **24**, 29-38 (2018).

15. Kerr, J.N., Greenberg, D. & Helmchen, F. Imaging input and output of neocortical networks in vivo. *Proc Natl Acad Sci U S A* **102**, 14063-14068 (2005).

16. Chen, T.W.*, et al.* Ultrasensitive fluorescent proteins for imaging neuronal activity. *Nature* **499**, 295-300 (2013).

17. Busche, M.A.*, et al.* Clusters of hyperactive neurons near amyloid plaques in a mouse model of Alzheimer's disease. *Science* **321**, 1686-1689 (2008).

18. Grienberger, C.*, et al.* Staged decline of neuronal function in vivo in an animal model of Alzheimer's disease. *Nat Commun* **3**, 774 (2012).

19. Busche, M.A.*, et al.* Decreased amyloid-β and increased neuronal hyperactivity by immunotherapy in Alzheimer's models. *Nat Neurosci* **18**, 1725-1727 (2015).

20. Keskin, A.D.*, et al.* BACE inhibition-dependent repair of Alzheimer's pathophysiology. *Proc Natl Acad Sci U S A* **114**, 8631-8636 (2017).

21. Jackson, R.J.*, et al.* Human tau increases amyloid-β plaque size but not amyloid beta-mediated synapse loss in a novel mouse model of Alzheimer's disease. *Eur J Neurosci* **44**, 3056-3066 (2016).

22. Santacruz, K.*, et al.* Tau suppression in a neurodegenerative mouse model improves memory function. *Science* **309**, 476-481 (2005).

23. Berger, Z.*, et al.* Accumulation of pathological tau species and memory loss in a conditional model of tauopathy. *J Neurosci* **27**, 3650-3662 (2007).

24. de Calignon, A.*, et al.* Caspase activation precedes and leads to tangles. *Nature* **464**, 1201-1204 (2010).

25. Angulo, S.L.*, et al.* Tau and amyloid-related pathologies in the entorhinal cortex have divergent effects in the hippocampal circuit. *Neurobiol Dis* **108**, 261-276 (2017).

26. Roberson, E.D.*, et al.* Reducing endogenous tau ameliorates amyloid β -induced deficits in an Alzheimer's disease mouse model. *Science* **316**, 750-754 (2007).

27. Ittner, L.M.*, et al.* Dendritic function of tau mediates amyloid-β toxicity in Alzheimer's disease mouse models. *Cell* **142**, 387-397 (2010).

28. DeVos, S.L.*, et al.* Antisense reduction of tau in adult mice protects against seizures. *J Neurosci* **33**, 12887-12897 (2013).

29. Zott, B., Busche, M.A., Sperling, R.A. & Konnerth, A. What happens with the circuit in Alzheimer's Disease in mice and humans? *Annu Rev Neurosci* **41**, 277-297 (2018).

30. Silverman, D.H.*, et al.* Positron emission tomography in evaluation of dementia: Regional brain metabolism and long-term outcome. *JAMA* **286**, 2120-2127 (2001).

31. Alexander, G.E., Chen, K., Pietrini, P., Rapoport, S.I. & Reiman, E.M. Longitudinal PET evaluation of cerebral metabolic decline in dementia: a potential outcome measure in Alzheimer's Disease treatment studies. *Am J Psychiatry* **159**, 738-745 (2002).

32. Greicius, M.D., Srivastava, G., Reiss, A.L. & Menon, V. Default-mode network activity distinguishes Alzheimer's disease from healthy aging: evidence from functional MRI. *Proc Natl Acad Sci U S A* **101**, 4637-4642 (2004).

33. Bradley, K.M.*, et al.* Cerebral perfusion SPET correlated with Braak pathological stage in Alzheimer's disease. *Brain* **125**, 1772-1781 (2002).

34. Jelic, V.*, et al.* Apolipoprotein E epsilon4 allele decreases functional connectivity in Alzheimer's disease as measured by EEG coherence. *J Neurol Neurosurg Psychiatry* **63**, 59-65 (1997).

35. Arriagada, P.V., Growdon, J.H., Hedley-Whyte, E.T. & Hyman, B.T. Neurofibrillary tangles but not senile plaques parallel duration and severity of Alzheimer's disease. *Neurology* **42**, 631-639 (1992).

36. Nelson, P.T.*, et al.* Correlation of Alzheimer disease neuropathologic changes with cognitive status: a review of the literature. *J Neuropathol Exp Neurol* **71**, 362-381 (2012).

37. Palop, J.J. & Mucke, L. Network abnormalities and interneuron dysfunction in Alzheimer disease. *Nat Rev Neurosci* **17**, 777-792 (2016).

38. Dickerson, B.C.*, et al.* Increased hippocampal activation in mild cognitive impairment compared to normal aging and AD. *Neurology* **65**, 404-411 (2005).

39. Bakker, A.*, et al.* Reduction of hippocampal hyperactivity improves cognition in amnestic mild cognitive impairment. *Neuron* **74**, 467-474 (2012).

40. Khan, U.A.*, et al.* Molecular drivers and cortical spread of lateral entorhinal cortex dysfunction in preclinical Alzheimer's disease. *Nat Neurosci* **17**, 304-311 (2014).

41. Hoover, B.R.*, et al.* Tau mislocalization to dendritic spines mediates synaptic dysfunction independently of neurodegeneration. *Neuron* **68**, 1067-1081 (2010).

42. Menkes-Caspi, N.*, et al.* Pathological tau disrupts ongoing network activity. *Neuron* **85**, 959-966 (2015).

43. Hatch, R.J., Wei, Y., Xia, D. & Gotz, J. Hyperphosphorylated tau causes reduced hippocampal CA1 excitability by relocating the axon initial segment. *Acta Neuropathol* **133**, 717-730 (2017).

44. Oddo, S.*, et al.* Reduction of soluble Abeta and tau, but not soluble Aβ alone, ameliorates cognitive decline in transgenic mice with plaques and tangles. *J Biol Chem* **281**, 39413-39423 (2006).

45. Sydow, A.*, et al.* Tau-induced defects in synaptic plasticity, learning, and memory are reversible in transgenic mice after switching off the toxic Tau mutant. *J Neurosci* **31**, 2511-2525 (2011).

46. Lasagna-Reeves, C.A.*, et al.* Tau oligomers impair memory and induce synaptic and mitochondrial dysfunction in wild-type mice. *Mol Neurodegener* **6**, 39 (2011).

47. Van der Jeugd, A.*, et al.* Cognitive defects are reversible in inducible mice expressing pro-aggregant full-length human tau. *Acta Neuropathol* **123**, 787-805 (2012).

48. Castillo-Carranza, D.L.*, et al.* Passive immunization with tau oligomer monoclonal antibody reverses tauopathy phenotypes without affecting hyperphosphorylated neurofibrillary tangles. *J Neurosci* **34**, 4260-4272 (2014).

49. Rudinskiy, N.*, et al.* Tau pathology does not affect experience-driven single-neuron and network-wide Arc/Arg3.1 responses. *Acta Neuropathol Commun* **2**, 63 (2014).

50. Kuchibhotla, K.V.*, et al.* Neurofibrillary tangle-bearing neurons are functionally integrated in cortical circuits in vivo. *Proc Natl Acad Sci U S A* **111**, 510-514 (2014).

FIGURE LEGENDS

Fig. 1. **Neuronal hyperactivity in APP/PS1 mice but silencing in rTg4510 tau mice.** (**a-c**) Top, *In vivo* two-photon fluorescence images of GCaMP6f-expressing (green) layer 2/3 neurons in the parietal cortex and corresponding activity maps from wild-type controls (a), APP/PS1 (b), and rTg4510 (c) mice. In APP/PS1 mice (b), plaques were labeled with methoxy-X04 (blue); in the activity maps neurons were color-coded as a function of their mean activity. Scale bars, 10 µm. Bottom, spontaneous Ca^{2+}-transients of neurons indicated in the top panel. (**d-f**) Frequency distributions of all recorded neurons in controls (d; green, *n* = 1705 neurons in 7 mice), APP/PS1 (e; magenta, *n* = 878 neurons in 5 mice), and rTg4510 mice (f; light blue, *n* = 1771 neurons in 9 mice). Dashed line at 6 transients per min indicates threshold used to identify hyperactive neurons; silent neurons exhibit 0 transients per min. (**g**) Mean neuronal frequencies for controls (1.69 ± 0.05 transients per min), APP/PS1 (3.42 ± 0.20 transients per min) and rTg4510 (0.66 ± 0.07 transients per min; $F(2,18) = 171.2$, $P = 1.93e\text{-}12$, all *post hoc* multiple comparisons between genotypes were highly significant: $P = 5.42e\text{-}9$ for controls vs. APP/PS1, $P = 1.38e\text{-}6$ for controls vs. rTg4510, P = 1.01e-12 for APP/PS1 vs. rTg4510). (**h,i**) Fractions of hyperactive neurons (h; controls: 2.91 ± 0.35 %, APP/PS1: 19.11 ± 1.50 %, rTg4510: 0.93 ± 0.35 %; $F(2,18) = 176.2$, $P = 1.51e\text{-}12$, *post hoc* multiple comparisons were $P = 2.84e\text{-}11$ for controls vs. APP/PS1, $P = 1.64e\text{-}12$ for APP/PS1 vs. rTg4510 and not significant, $P = 0.1045$, for controls vs. rTg4510) as well as silent neurons (i; controls: 15.05 ± 1.87 %, APP/PS1: 9.20 ± 2.36 %, rTg4510: 53.48 ± 3.24 %; $F(2,18) = 77.18$, $P = 1.48e\text{-}9$, *post hoc* multiple comparisons were $P = 2.02e\text{-}8$ for controls vs. rTg4510 and $P = 1.08e\text{-}8$ for APP/PS1 vs. rTg4510 and not significant, $P = 0.3972$, for controls vs. APP/PS1). Each solid circle represents an individual animal (controls, *n* = 7; APP/PS1, *n* = 5;

rTg4510, *n* = 9) and all error bars reflect mean ± s.e.m; differences between genotypes were assessed by one-way ANOVA followed by Tukey's multiple comparisons test, ****P < 0.0001, n.s., not significant.

Fig. 2. NFTs are not required for neuronal silencing. (**a**) Coronal sections showing many Alz50 (top panel, green) and PHF-1 (bottom panel, red) positive NFTs in the cortex of rTg4510 mice (*n* = 4 mice, 8 - 10 sections per mouse were analyzed), but not in rTg21221 mice (*n* = 4 mice, 5 - 12 sections per mouse were analyzed). Nuclei are visualized with DAPI (blue). Scale bars, 100 µm. (**b**) *In vivo* two-photon fluorescence images of GCaMP6f-expressing (green) layer 2/3 neurons and corresponding activity maps from 3 example rTg21221 mice illustrating the marked silencing of many neurons. Scale bars, 10 µm. (**c**) Frequency distributions of all recorded neurons in wild-type controls (left panel, green, *n* = 1705 neurons in 7 mice) and rTg21221 mice (right panel, orange, *n* = 1021 neurons in 6 mice). (**d,e**) Summary graphs representing mean frequencies (d; controls: 1.69 ± 0.05 transients per min, rTg4510: 0.66 ± 0.07 transients per min, rTg21221: 1.07 ± 0.11 transients per min; F(2,19) = 48.43, *P* = 3.47e-8, all *post hoc* multiple comparisons between genotypes were significant: *P* = 2.01e-8 for controls vs. rTg4510, *P* = 1.00e-4 for controls vs. rTg21221, *P* = 0.0038 for rTg4510 vs. rTg21221) and fractions of silent neurons (e; controls: 15.05 ± 1.87 %, rTg4510: 53.48 ± 3.24 %, rTg21221: 40.25 ± 3.64 %; F(2,19) = 42.94, *P* = 8.94e-8, all *post hoc* multiple comparisons between genotypes were significant: *P* = 5.55e-8 for controls vs. rTg4510, *P* = 7.85e-5 for controls vs. rTg21221, *P* = 0.0179 for rTg4510 vs. rTg21221). Data for controls and rTg4510 are the same as in Fig. 1. Each solid circle

represents an individual animal and all error bars reflect mean ± s.e.m; differences between genotypes were assessed by one-way ANOVA followed by Tukey's multiple comparisons test, ****P < 0.0001, **P < 0.01, *P < 0.05.

Fig. 3. **No hyperactivity and many silent neurons in mice harboring both tau and Aβ.** (**a-c**) Coronal sections showing coexistence of NFTs (green) and Aβ plaques (red) in the cortex of APP/PS1-rTg4510 mice (b), but only plaques in APP/PS1 (a) and APP/PS1-rTg21221 (c) mice. Immunostainings were repeated independently in multiple animals (APP/PS1, *n* = 7; APP/PS1-rTg4510, *n* = 15; APP/PS1-rTg21221, *n* = 13) with similar results. Scale bars, 100 µm. (**d,e**) Top, *In vivo* two-photon fluorescence images of layer 2/3 neurons and corresponding activity maps from APP/PS1-rTg4510 (d) and APP/PS1-rTg21221 (e) mice. Methoxy-X04-labeled plaques are shown in blue. Bottom, spontaneous Ca^{2+}-transients of neurons indicated in top panel. Scale bars, 20 µm. (**f-h**) Frequency distribution of all recorded neurons in APP/PS1 (f, *n* = 878 neurons in 5 mice), APP/PS1-rTg4510 (g, *n* = 2092 neurons in 9 mice) and APP/PS1-rTg21221 mice (h, *n* = 1050 neurons in 5 mice). (**i-k**) Summary graphs representing mean frequencies (i; APP/PS1: 3.42 ± 0.20 transients per min, APP/PS1-rTg4510: 0.52 ± 0.09 transients per min, APP/PS1-rTg21221: 1.16 ± 0.14 transients per min; $F(2,15) = 119.9$, $P = 5.96e\text{-}10$, all *post hoc* multiple comparisons between genotypes were significant: $P = 4.36e\text{-}10$ for APP/PS1 vs. APP/PS1-rTg4510, $P = 5.64e\text{-}8$ for APP/PS1 vs. APP/PS1-rTg21221, $P = 0.012$ for APP/PS1-rTg4510 vs. APP/PS1-rTg21221), fractions of hyperactive neurons (j; APP/PS1: 19.11 ± 1.50 %, APP/PS1-rTg4510: 1.00 ± 0.43 %, APP/PS1-rTg21221: 4.25 ± 1.13 %; $F(2,15) = 98.35$, $P = 2.39e\text{-}9$, *post hoc* multiple comparisons

were highly significant, *P* = 2.02e-9, for APP/PS1 vs. APP/PS1-rTg4510 as well as APP/PS1 vs. APP/PS1-rTg21221 (*P* = 1.21e-7) but not significant, *P* = 0.065, for APP/PS1-rTg4510 vs. APP/PS1-rTg21221) as well as silent neurons (k; APP/PS1: 9.20 ± 2.36 %, APP/PS1-rTg4510: 62.61 ± 2.56 %, APP/PS1-rTg21221: 44.47 ± 4.10 %; *F*(2,15) = 80.86, *P* = 9.25e-9, all *post hoc* multiple comparisons between genotypes were significant: *P* = 5.72e-9 for APP/PS1 vs. APP/PS1-rTg4510, *P* = 4.87e-6 for APP/PS1 vs. APP/PS1-rTg21221, *P* = 0.002 for APP/PS1-rTg4510 vs. APP/PS1-rTg21221). Data for APP/PS1 mice are the same as shown in Fig. 1. Each solid circle represents an individual animal and all error bars reflect mean ± s.e.m; differences among genotypes were assessed by one-way ANOVA followed by Tukey's multiple comparisons test, ****P < 0.0001, **P < 0.01, *P < 0.05, n.s., not significant.

Fig. 4. **Tau transgene suppression rescues neuronal silencing in tau mice but not in mice with tau and Aβ.** (**a,b**) Example activity traces from neurons before (black) and after (red) tau suppression with doxycycline (DOX) in the same rTg4510 (a) and APP/PS1-rTg4510 (b) mice. (**c,d**) Frequency distributions of all recorded neurons from rTg4510 mice (c) before (baseline, *n* = 1412 neurons in 7 mice) and after (*n* = 1118 neurons in same 7 mice) DOX. The same is shown for rTg21221 mice (d) (before DOX, *n* = 1675 neurons in 8 mice; after DOX, *n* = 1036 neurons in same 8 mice) (**e**) Fractions of silent neurons in rTg4510 (left; *n* = 7 mice) and rTg21221 (right; *n* = 8 mice) before and after DOX (rTg4510, before DOX: 50.84 ± 3.49 % vs. after Dox: 25.92 ± 2.57 %, *t* = 5.753, *d.f.* = 11.03, *P* = 1.26e-4; rTg21221, before DOX: 40.45 ± 3.68 % vs. after DOX: 15.87 ± 1.74 %, *t* = 6.047, *d.f.* = 9.972, *P* = 1.26e-4). (**f,g**) Frequency distributions from APP/PS1-

rTg4510 mice (f) before (*n* = 1262 neurons in 5 mice) and after (*n* = 827 neurons in same 5 mice) DOX. The same is shown for APP/PS1-rTg21221 mice (g, before DOX, *n* = 795 neurons in 5 mice; after DOX, *n* = 904 neurons in same 5 mice). (**h**) Fractions of silent neurons in APP/PS1-rTg4510 (left; *n* = 5 mice) and APP/PS1-rTg21221 (right; *n* = 5 mice) before and after DOX (APP/PS1-rTg4510, before DOX: 64.25 ± 4.21 % vs. after DOX: 61.87 ± 2.28 %, *t* = 0.4962, *d.f.* = 6.152, *P* = 0.6370; APP/PS1-rTg21221, before DOX: 44.72 ± 4.59 % vs. after DOX: 46.04 ± 2.64 %, *t* = 0.2494, *d.f.* = 6.387, *P* = 0.8109; two-sided *t*-test). Each solid circle represents an individual animal and error bars represent mean ± s.e.m., differences among groups were assessed using two-sided *t*-test, ***P < 0.001, n.s., not significant.

METHODS

Animals: Generation, care and use of the animals as well as all experimental procedures were approved by the Massachusetts General Hospital's and McLaughlin Research Institute's Institutional Animal Care and Use Committees. All mice were housed in standard mouse cages on wood bedding under conventional laboratory conditions (12-h dark and 12-h light cycle, constant temperature and constant humidity), and food and water *ad libitum*. Male and female mice were used in the study and randomly allocated to the experiments. B6.Cg-Tg(APPswe, PSEN1dE9)85Dbo/MmJ mice (hereafter designated APP/PS1) were initially obtained from Jackson Laboratory (Bar Harbor, ME)[51]. APP/PS1 mice were crossed to the B6.Cg-Tg(Camk2a-tTA)1/Mmay tet transactivator strain that expresses tTA from the CK-tTA transgene exclusively in the forebrain[52]. Double transgenic B6.CK-tTA, APP/PS1 males were selected as sires for the experimental cross to dams from the tetracycline-responsive element strain FVB-Tg(tetO-MAPT*P301L)4510/Kha/Jlws (Tg4510) or FVB-Tg(tetO-MAPT*wt)21221 (Tg21221) to produce APP/PS1-rTg4510 or APP/PS1-rTg21221 mice with the experimental, tau-expressing genotypes plus mice negative for either the responder or transactivator transgene that do not express any human tau. All of the same sex offspring of these crosses share the FVBB6F1 background and are genetically identical to one another except for the transgene arrays that they carry.

Surgery and injection of genetically encoded Ca^{2+}-indicator: Mice were initially anesthetized with 4 % isoflurane in O_2 and maintained on 2 % isoflurane during the surgical procedure. The body temperature of the anesthetized mice was maintained at ~37.5°C using a heating pad, and ophthalmic ointment was applied to protect the eyes. Using aseptic techniques, the skin above

the skull was removed and, by using a fine-tipped dental drill, two craniotomies were performed over both the left and right parietal cortices. Then the fast and sensitive genetically encoded fluorescent Ca^{2+}-sensor GCaMP6f[16] (AAV1.Syn.GCaMP6f.WPRE.SV40; purchased from UPenn Vector Core), was stereotactically (Kopf Instruments) injected into layer 2/3 (~300 µm deep) at a rate of 0.2 µl per min using a microsyringe pump (Harvard Apparatus, Pump 11 Elite). A single injection (~1 µl of viral construct) was made in each cortical hemisphere. A round glass coverslip (8 mm diameter) was placed over both craniotomies and sealed to the bone using a mix of dental cement and cyanoacrylate[50]. After surgery mice were returned to their home cage for 2 to 3 weeks. Analgesia (buprenorphine and acetaminophen) was continued for 3 d postoperatively.

***In vivo* two-photon fluorescence microscopy:** To minimize brain state-dependent experimental variables[53] and for better comparison with previous studies[17-20], imaging was performed under light isoflurane anesthesia in the present study. Mice were anesthetized with 4 % isoflurane in O_2 for induction, and a reduced concentration of isoflurane (~1 %) was used during the imaging. After induction, we waited at least 60 min before imaging. The animal´s body temperature was maintained at ~37.5°C with a heating pad, and ophthalmic ointment was applied to protect the eyes. Two-photon imaging was performed on an Olympus FluoView1000 microscope equipped with a mode-locked Ti:sapphire laser (MaiTai, Spectra Physics) tuned to 900 nm. Spontaneous Ca^{2+}-fluorescence signals from cortical layer 2/3 were recorded at ~15 Hz through a 25x, 1.05 numerical aperture water immersion objective (Olympus, 6X digital zoom). Scanning and image acquisition was controlled by the Fluoview software (Olympus). Imaging was carried-out across

multiple fields of view (256 x 256 pixels, 84.41 x 84.41 µm) per mouse, and each field of view was recorded for at least 130 s. Image analysis was performed offline using the Fiji package of ImageJ (National Institutes of Health) and Igor Pro (Wavemetrics). First, regions of interest (ROIs) were drawn around individual neuronal somata, and then relative GCaMP6f fluorescence change versus time traces were generated for each ROI. Ca^{2+}-transients were identified as changes in relative fluorescence that were three times larger than the standard deviation of the baseline fluorescence. Based on previous protocols[19, 20], neurons were classified according to their individual activity rates as silent (0 transients per min), normal (0-6 transients per min) or hyperactive (≥6 transients per min).

Immunohistochemistry: Brain hemispheres from mice were drop fixed in 4 % paraformaldehyde (PFA) in PBS for 48 h at 4° C. After fixation, brains were washed with PBS, cryoprotected with 30 % sucrose and sliced into 40-µm-thick coronal sections (Leica SM2000 R). Sections were rinsed three times in TBS and then permeabilized with 0.2 % Triton X-100 in TBS for 20 minutes. Sections were then blocked in 10 % normal goat serum (NGS) in TBS for 60 minutes at room temperature, followed by overnight incubation at 4°C in primary antibodies diluted in 5 % NGS. The following primary antibodies were used: mouse anti-Alz50 IgM (1:500, courtesy of Peter Davies), chicken anti-GFP (1:1000, Aves Labs, cat. no. GFP-1020), rabbit anti-human Aβ (1:500, IBL America, cat. no. 18584), mouse anti-PHF1 IgG (1:1000, courtesy of Peter Davies). After three washes in TBS, sections were incubated in secondary antibodies diluted in 5 % NGS for 60 minutes at room temperature. After three washes in TBS, sections were incubated in secondary antibodies diluted in 5 % NGS for 60 minutes at room temperature. The

following secondary antibodies were used: goat anti-mouse IgM cy3 (1:1000, Millipore, cat. no. AP128C), Alexa Fluor488 goat anti-chicken (1:1000, Invitrogen, cat. no. A11039), Alexa Fluor647 goat anti-rabbit (1:500, Invitrogen, cat. no. A21245), Alexa Fluor647 goat anti-mouse IgG (1:500, Invitrogen, cat. no. A21235). After three washes in TBS, sections were mounted on microscope slides in DAPI fluoromount (VectaShield) and coverslipped. Images were recorded on a Zeiss Axio-Imager microscope equipped with a Coolsnap digital camera and Axio-Vision V4.8. Stereological quantifications of NFTs and amyloid plaques were performed using the Computer Assisted Stereological Toolbox (Olympus). All counting was conducted blinded to genotype and treatment. Further information about antibodies used for immunohistochemistry can be found in the Life Sciences Reporting Summary.

Tau protein analysis: Mouse forebrain was homogenized with a dounce homogenizer in 300 µL PBS with protease inhibitor (100:1, Thermo Scientific) and spun at 10,000 g for 10 minutes at 4^{o}C. The pellet was collected for sarkosyl extraction. Protein concentration was determined with a bicinchoninic acid assay (BCA, Thermo Scientific Pierce). Enzyme-Linked Immunosorbent Assays (ELISA) were performed using the Meso Scale Diagnostics (MSD) Phospho (Thr231)/Total Human Tau ELISA kit (MSD #K15121D), per the manufacturer's protocol. All samples were run in duplicate and fit to an eight-point standard curve for concentration determination. For sarkosyl soluble/insoluble tau isolation, the same protein quantity of mouse brain lysate pellet was resuspended in cold TBS and centrifuged at 150,000 x g, 15 min, 4^{o}C. The pellet was then homogenized in 3x salt/sucrose buffer (0.8M NaCl, 10% sucrose, 10mN Tris-base pH 7.4) and centrifuged at 150,000 x g, 15 min, 4^{o}C. The supernatant was collected, adjusted to 1% sarkosyl

and incubated 1h at 37°C. Samples were then centrifuged at 150,000 x g, 30 min, 4°C. Supernatant and pellets were collected. Pellets were resuspended with RIPA buffer containing 1% SDS and sonicated for 20 min in a bath sonicator (Branson 2510). Both supernatant (sarkosyl soluble) and pellets (sarkosyl insoluble) were then analyzed by Western blot as follows: sarkosyl-soluble and insoluble fractions were mixed with 1x final LDS sample buffer (Invitrogen) and 50mM DTT (10x sample Reducing agent, Invitrogen), and boiled for 5 minutes. Samples were loaded in 4-12% Bis-Tris gel (Invitrogen) and run at 130V for 90 minutes in 1x MES SDS running buffer (Invitrogen). Proteins were then transferred to an activated polyvinylidene fluoride membrane (EMD Millipore) in 1x transfer buffer (Bio-rad) at 75V for 75 minutes. Membranes were then blocked for 1 hour using Odyssey blocking buffer (LI-COR) at room temperature and then incubated with a mouse anti-human Tau antibody (Tau-13, 1:2500 - Biolegend) and a chicken anti-GAPDH antibody (1:5000, Millipore) in LI-COR blocking buffer overnight at 4°C. Membranes were then washed 3x10min in Tris-buffered saline with Tween 20 (TBS-T), and then incubated with secondary antibodies (goat anti-mouse IgG IRDye680RD, Donkey anti-chicken IgG IRDye800CW, LICOR) for 1 hour at room temperature. Membranes were imaged using a LI-COR imaging station using the Odyssey software. Blots were converted to greyscale and densitometry analysis performed in ImageJ. Further information about the antibodies used for tau protein analysis can be found in the Life Sciences Reporting Summary.

Statistics: No statistical methods were used to pre-determine sample sizes but our sample sizes are similar to those reported in previous publications (see, e.g., refs. [17-20]). No animals or data points were excluded from the analysis. Biochemical and histological analyses were conducted

blinded to genotype and treatment, whereas *in vivo* microscopy and analysis were not performed blinded to the conditions of the experiments. The distributions of firing rates of neurons were analyzed using linear mixed effects models with animal as a random factor, and fixed factors as stated in the main text. Since the distributions of firing rates were highly skewed to the right, a log transformation was used to ensure normality (this was the best Box-Cox transformation for these data). Firing rates of 0 were coded as half the lowest non-zero observed rate before the log transformation. Computations were performed using the function fitlme in the statistical toolbox of Matlab R2017b (Mathworks). Statistical comparison between two experimental groups was assessed by two-sided *t*-test, and differences between multiple groups were assessed using one-way ANOVA followed by Tukey's multiple comparisons test. $P < 0.05$ was considered statistically significant. Analysis routines and code used in this study are available from the corresponding authors upon request.

DATA AVAILABILITY

All data are reported in the main text and supplementary materials, stored at the Massachusetts General Hospital and are available from the corresponding authors upon reasonable request.

METHODS-only REFERENCES

51. Jankowsky, J.L.*, et al.* Mutant presenilins specifically elevate the levels of the 42 residue β-amyloid peptide in vivo: evidence for augmentation of a 42-specific gamma secretase. *Hum Mol Genet* **13**, 159-170 (2004).

52. Mayford, M.*, et al.* Control of memory formation through regulated expression of a CaMKII transgene. *Science* **274**, 1678-1683 (1996).

53. Froudarakis, E.*, et al.* Population code in mouse V1 facilitates readout of natural scenes through increased sparseness. *Nat Neurosci* **17**, 851-857 (2014).

Figure 1

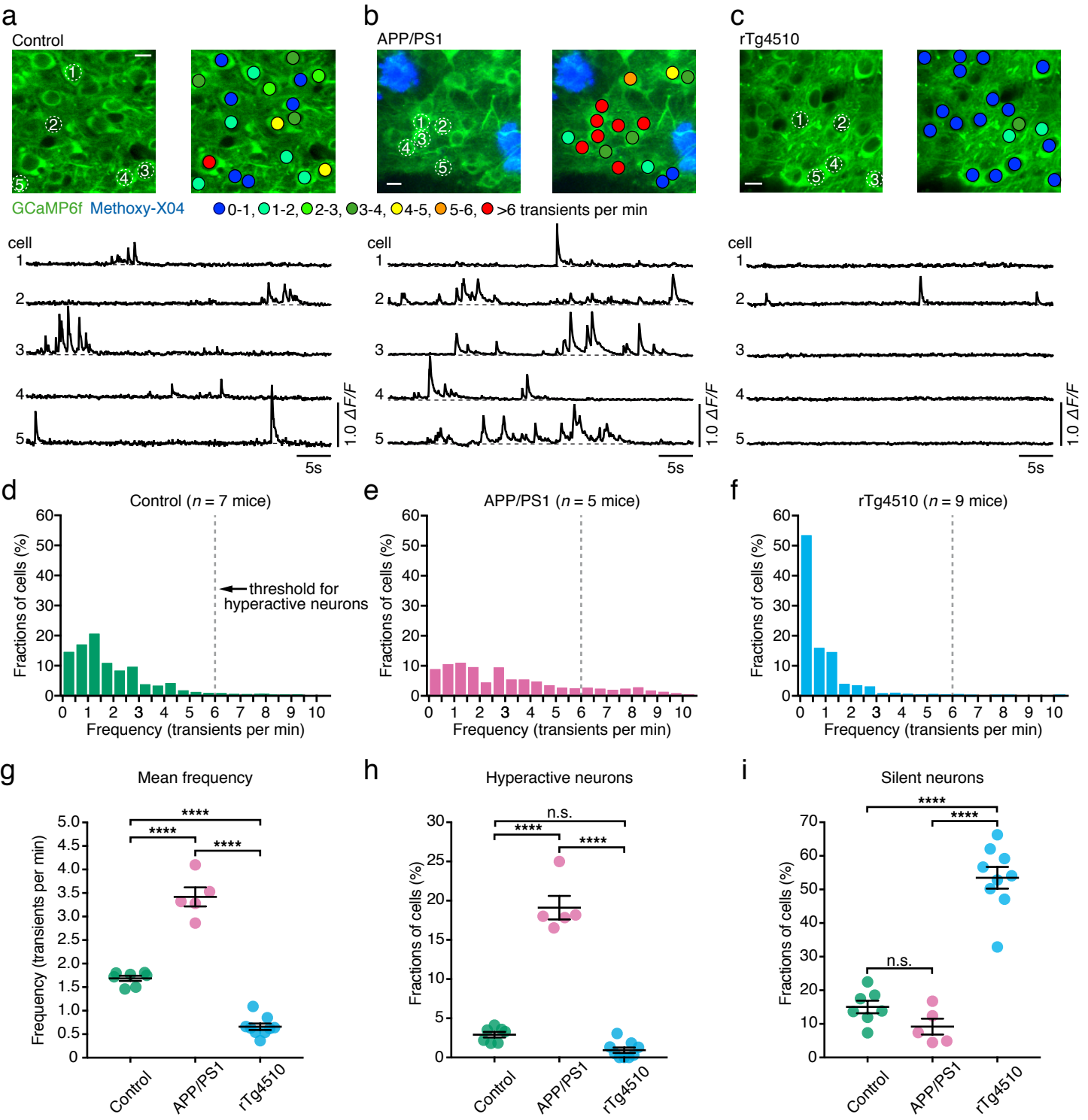
a
Control
b
APP/PS1
c
rTg4510
GCaMP6f Methoxy-X04
0-1, 1-2, 2-3, 3-4, 4-5, 5-6, >6 transients per min
cell
1.0 ΔF/F
5s
d
Control (n = 7 mice)
threshold for hyperactive neurons
Fractions of cells (%)
Frequency (transients per min)
e
APP/PS1 (n = 5 mice)
f
rTg4510 (n = 9 mice)
g
Mean frequency
Frequency (transients per min)
****
h
Hyperactive neurons
n.s.
i
Silent neurons
Control
APP/PS1
rTg4510

Figure 2

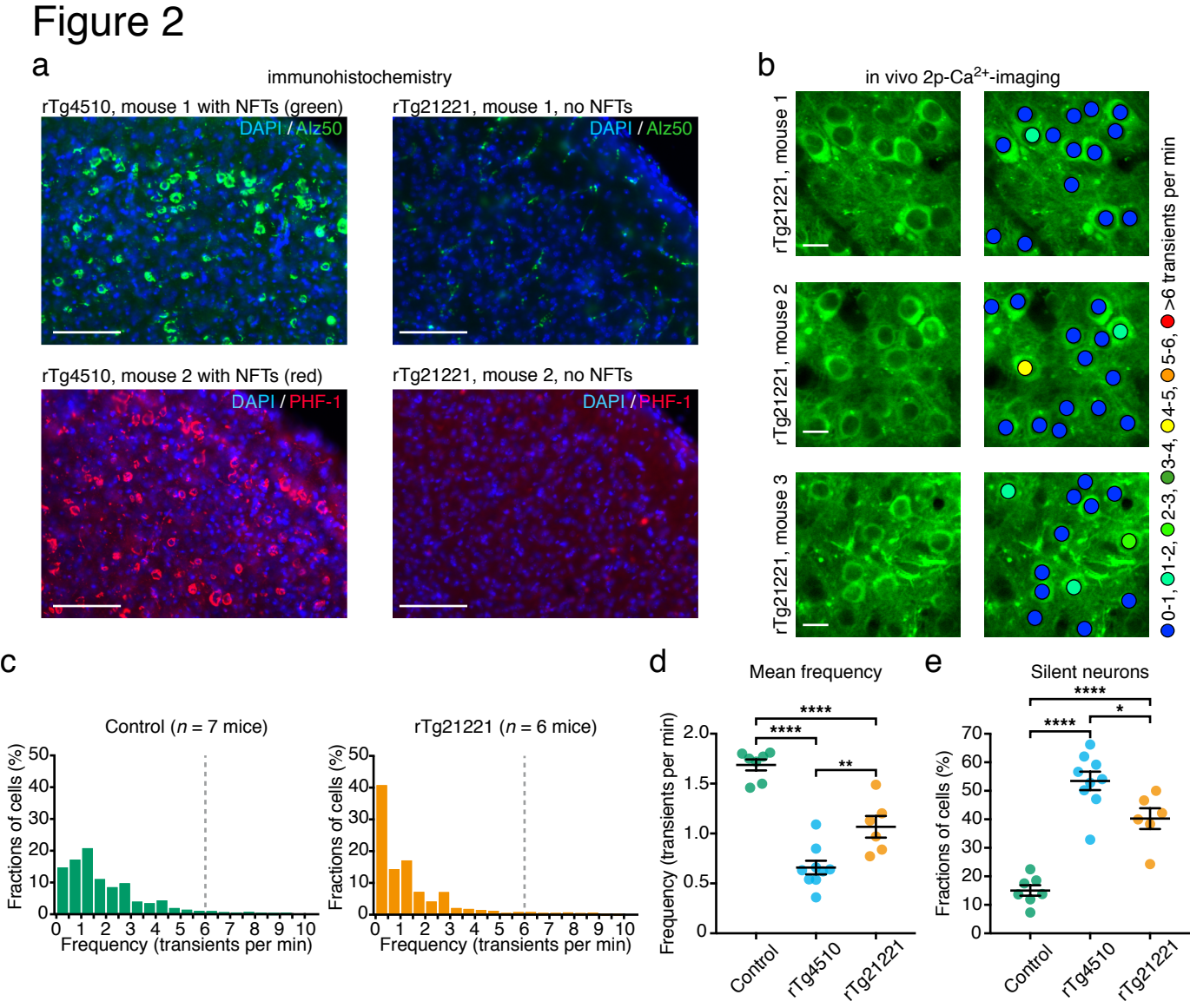
a
immunohistochemistry
rTg4510, mouse 1 with NFTs (green)
DAPI / Alz50
rTg21221, mouse 1, no NFTs
DAPI / Alz50
rTg4510, mouse 2 with NFTs (red)
DAPI / PHF-1
rTg21221, mouse 2, no NFTs
DAPI / PHF-1
b
in vivo 2p-Ca2+-imaging
rTg21221, mouse 1
rTg21221, mouse 2
rTg21221, mouse 3
0-1, 1-2, 2-3, 3-4, 4-5, 5-6, >6 transients per min
c
Control (n = 7 mice)
rTg21221 (n = 6 mice)
Fractions of cells (%)
Frequency (transients per min)
d
Mean frequency
Frequency (transients per min)
Control
rTg4510
rTg21221
e
Silent neurons
Fractions of cells (%)
Control
rTg4510
rTg21221

Figure 3

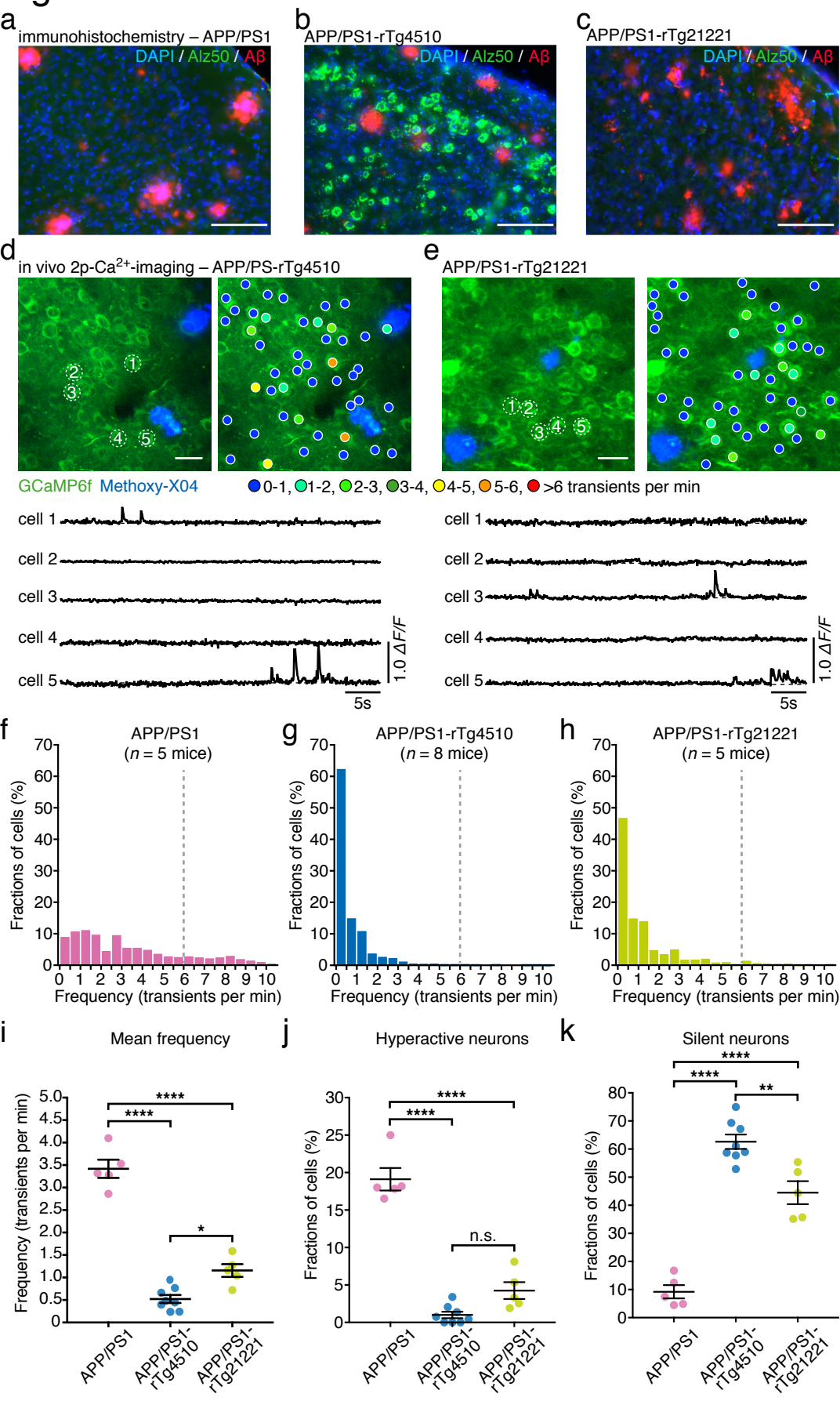
a
immunohistochemistry – APP/PS1
DAPI / Alz50 / Aβ
b
APP/PS1-rTg4510
DAPI / Alz50 / Aβ
c
APP/PS1-rTg21221
DAPI / Alz50 / Aβ
d
in vivo 2p-Ca2+-imaging – APP/PS-rTg4510
e
APP/PS1-rTg21221
GCaMP6f Methoxy-X04
0-1, 1-2, 2-3, 3-4, 4-5, 5-6, >6 transients per min
cell 1
cell 2
cell 3
cell 4
cell 5
1.0 ΔF/F
5s
f
APP/PS1
(n = 5 mice)
g
APP/PS1-rTg4510
(n = 8 mice)
h
APP/PS1-rTg21221
(n = 5 mice)
Fractions of cells (%)
Frequency (transients per min)
i
Mean frequency
Frequency (transients per min)
j
Hyperactive neurons
Fractions of cells (%)
n.s.
k
Silent neurons
Fractions of cells (%)
APP/PS1
APP/PS1-rTg4510
APP/PS1-rTg21221

Figure 4

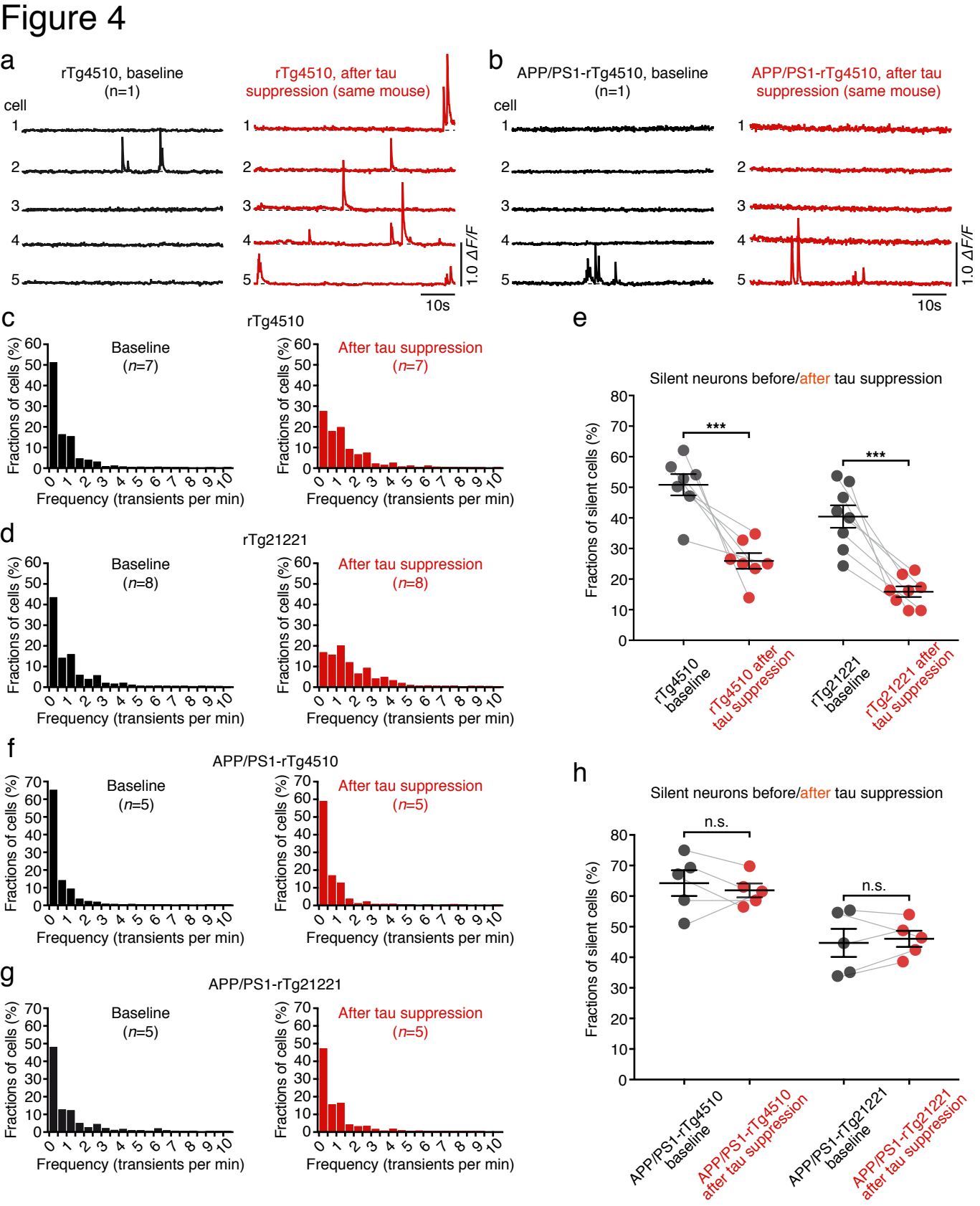
a
rTg4510, baseline
(n=1)
rTg4510, after tau
suppression (same mouse)
cell
1
2
3
4
5
1.0 ΔF/F
10s
b
APP/PS1-rTg4510, baseline
(n=1)
APP/PS1-rTg4510, after tau
suppression (same mouse)
cell
1.0 ΔF/F
10s
c
rTg4510
Baseline
(n=7)
After tau suppression
(n=7)
Fractions of cells (%)
Frequency (transients per min)
d
rTg21221
Baseline
(n=8)
After tau suppression
(n=8)
e
Silent neurons before/after tau suppression
Fractions of silent cells (%)
***
***
rTg4510
baseline
rTg4510 after
tau suppression
rTg21221
baseline
rTg21221 after
tau suppression
f
APP/PS1-rTg4510
Baseline
(n=5)
After tau suppression
(n=5)
g
APP/PS1-rTg21221
Baseline
(n=5)
After tau suppression
(n=5)
h
Silent neurons before/after tau suppression
n.s.
n.s.
APP/PS1-rTg4510
baseline
APP/PS1-rTg4510
after tau suppression
APP/PS1-rTg21221
baseline
APP/PS1-rTg21221
after tau suppression